Robotica (2022), **40**, pp. 2468–2484
doi:10.1017/S0263574721001740

CAMBRIDGE
UNIVERSITY PRESS

RESEARCH ARTICLE

Design, modeling, and testing of a soft actuator with variable stiffness using granular jamming

Junfeng Hu*, Long Liang and Bin Zeng

School of Mechanical and Electrical Engineering, Jiangxi University of Science and Technology, Ganzhou, China
*Corresponding author. E-mail: hjfsuper@126.com

Received: 6 September 2019; **Revised:** 24 September 2021; **Accepted:** 29 October 2021;
First published online: 7 February 2022

Keywords: soft actuator, variable stiffness, granular jamming, heavy-load actuator

Abstract

Soft robots combine the load-bearing capability of rigid material with the resilience, shape-shifting capabilities of soft materials. This paper presents a novel soft actuator with stiffness variation using particulate jamming technology. We design a hybrid composite structure consisting of driving layer and jamming layer. The driving layer with the arc air chamber aim to achieve large bending deformation. A membrane containing particles is integrated with driving layer to module its stiffness. The influence factors of stiffness variation were analyzed from energy of point of view. The dependence of granular attributes on the stiffness of the actuator was studied. Furthermore, we illustrated influence of stiffness changes on the kinematic and dynamic performance of the soft actuator. The experimental results showed these performance indexes are twofold. On the one hand, the structural parameters have significant effect on the bending angle, but on the other hand they have little effect on the end force. We found that flow resistance inside air chamber results in bending morphology variation. The dynamic response subjected to a square-wave air pressure was analyzed to exhibit the actuator's transient and steady vibration behavior. The actuator with greater stiffness has faster responsiveness, but smaller range of motion. These conclusions are helpful to adjust the stiffness behavior and to improve motion performance.

1. Introduction

The flexible actuator [1] has attracted a lot of attention over the past decade. The proliferation of soft robotics research worldwide has brought substantial achievements in principles, models, technologies, techniques, and soft robot prototypes [2, 3]. The soft actuator [4] has the advantages of self-adaptation, light and safe, low-cost rapid design, and production. It has attracted extensive attention in the fields of biomedicine, industrial production, and deep-sea exploration. Although soft actuators have high compliance and security, soft actuators' inherent low stiffness limits their ability to perform tasks that require relatively high load capacity. Variable stiffness is an effective way to solve this problem. By changing the stiffness, the soft actuator can make the stiffness change as needed. Case Western Reserve University has developed an origami-based three-finger manipulator with potential applications for effective manipulation of fragile objects [5]. Tufts University has put forward a design and manufacturing method to create a motor tendon-actuated soft foam robot [6]. The Zhejiang University of Technology has presented a pneumatic trunk-like soft actuator, adjusting the stiffness and realizing the omni-directional bending motion [7]. Common soft actuators are designed as monolithic structures from soft materials, such as silicone rubbers, electroactive polymers, shape memory alloys, elastomers, hydrogels, or composites. But these soft materials enable it inherent low stiffness. Therefore, we need to study how to integrate variable stiffness structure into one with soft materials.

Various variable stiffness methods have been investigated to resolve the issue of low intrinsic stiffness of soft robots. At present, there are at least two methods for changing the stiffness of a soft actuator. The

first method is to use new material to change stiffness, such as a magnetorheological material, a thermally adjustable composite material, a shape memory material, [8, 9] a low-melting alloy material, [10, 11] and the like. Harvard University has developed a stiffness-adjustable elastomer with a micro-magneto-flow domain under a low magnetic field using magnetorheological materials [12]. MIT uses a new thermally tunable composite material to achieve stiffness changes in the actuator [13]. The University of Science and Technology of Singapore designed a 3D-printed stiffness-adjustable soft actuator using shape memory polymer materials [14]. Johns Hopkins University has proposed a cable-driven, stiffness-adjustable continuum manipulator using a low-melting alloy material [15]. However, materials to achieve stiffness changes have the disadvantages of slow response and high cost.

The second method is jamming technology. The technique utilizes the jamming phenomenon to implement a reversal phase transition between a fluid-like and a solid-like material. There are two jamming methods, including granular jamming [16, 17] and laminar jamming [18, 19]. Brown et al. developed a universal clamp with variable stiffness based on granular jamming technology [20, 21]. The Delft University of Technology designed a flexible endoscope based on granular jamming technology [22]. The Massachusetts Institute of Technology has developed a variable-spinning serpentine manipulator using laminar jamming technology [23]. Wang Tao et al. designed a soft flexible soft robot using electrostatic layer jamming technology [24]. Compared with laminar jamming, granular jamming has a simple structure, an extensive range of stiffness variation, and large deformation in a fluid state. Due to these factors, granular jamming is considered more practical than laminar one. The jamming transition phenomenon is widely employed to vary stiffness due to its simplicity, low cost, versatility, and fast response. Jamming is the mechanism by which particle material can transition between a liquid-like and a solid-like state [25]. The jamming can be achieved with a small change in confining volume of the granular material, for instance, through application of a vacuum. Though jamming itself can do no net external work on the environment to enable mobility, it can modulate the work performed by another actuator. These effects of factors on particle jamming technique have been analyzed in previous literature. But the impact of these factors on soft actuator was not illustrated. Meanwhile, we need to demonstrate the dynamic feature of the soft actuator with stiffness variation.

Soft actuators with integrated particle jamming have been reported in the literatures [26, 27]. Li proposed an actuator using a passive particle jamming principle that does not need vacuum pressure [26]. The soft actuator consists of a driving structure with silicone rubber and a pack of particles integrated in the soft driving structure. The particles inside a pack squeeze together under an external air pressure causing the stiffness increases. But this particle jamming actuation method is different from vacuum jamming, and the stiffness is dependent on the bending degree of the soft actuator. Besides vacuum-based particle jamming, there are alternative particle jamming methods. Rheology theory can be used to describe particle jamming mechanism. Particles responding to specific external electric or magnetic rearrange in a medium inside a confined space or volume, such as air, fluid, emulsion, foam, or elastomer. The interaction force between particles induced by the physical fields enables them to squeeze together causing the stiffness increases. However, the soft actuator based on this principle requires high electric or magnetic fields. To avoid these drawbacks, we design a hybrid composite structure consisting of driving layer and jamming layer. The driving layer with the arc air chamber aim to achieve large bending deformation. A membrane containing particles is integrated with driving layer to module its stiffness by air negative pressure.

Contributions of the presented research can be highlighted as a hybrid composite soft actuator. The dependence of granular attributes on the stiffness of the actuator is illustrated. Furthermore, the influence of particles on the kinematic and dynamic performance of the soft actuator is explored. Meanwhile, the bending morphology variation is exploited due to flow resistance inside air chamber. And the actuator's transient and steady vibration behavior is exhibited.

This paper is organized as follows. In Section 2, a new soft actuator with stiffness variation is proposed using granular jamming technology, and we give the fabrication process of the prototype of the actuator. The mechanical model reflecting the bending property of the actuator is established, and the bending performance is analyzed in Section 3. In Section 4, the factors affecting the stiffness of the actuator are

https://doi.org/10.1017/S0263574721001740 Published online by Cambridge University Press

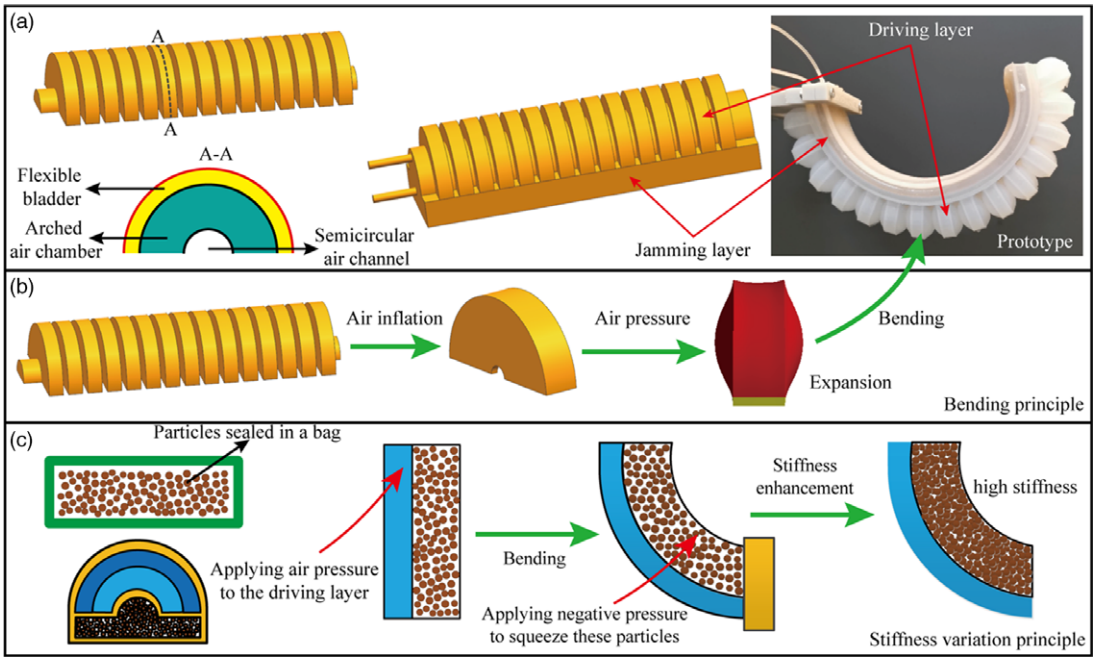

Figure 1. *Structure and working principle of the soft actuator. (a) Design of soft actuator. (b) Bending principle. (c) Stiffness variation principle.*

explored through the experimental test, and the advantage of stiffness variation is illustrated by carrying out load capacity and grabbing trial. Section 5 concludes this paper.

2. Design of soft actuator

2.1. Structural design

Pneumatic actuator function by networks of elastomeric channels that inflate upon pressurization. Though multiple soft actuators exist, they have not been utilized to their full extent in a soft robot due to inherent flexibility. A solution was presented herein that relies on a rigidity change in a granular material jamming that allows a material to transition from a liquid-like state to a solid-like state. As shown in Fig. 1(a), a two-layer pneumatic actuator comprises a driving layer and a jamming layer. The driving layer can bend by air pressure, and the jamming layer is to achieve stiffness variation. As shown in Fig. 1(a), the driving layer structure is an extendable layer consisting of several equally spaced inflatable airbags. The inflated airbag is an arched air chamber with semicircular air channels. The bending principle of the actuator is illustrated in Fig. 1(b). When the driving layer is inflated and pressurized, the airbag expands and deforms under the action of air pressure. Furthermore, the jamming layer does not produce telescopic deformation. The actuator can achieve a bending deformation. At rest state, there is no pressure difference between the inside and the outside of the airbag. When actuated by air pressure, the bending angle of the driving layer is dependent on the pressure difference. Although the actuator can achieve good bending properties, the stiffness of the soft actuators cannot be varied a lot given a low pneumatic. So, a jamming layer sealed with a pack of particles is designed to achieve it.

The jamming layer is comprised of the flexible membrane that encloses many granules. The flexible membrane contains particles that can be jammed by applying a vacuum or unjammed by releasing it. The jamming granules loosely distribute in the cavity under vacuum off. The jamming granules are freely movable in the niche due to external force, exhibiting a flowing state. The rigidity of the jamming layer is low. In the vacuum state, the jamming granules densely distribute in the cavity. The jamming granules

https://doi.org/10.1017/S0263574721001740 Published online by Cambridge University Press

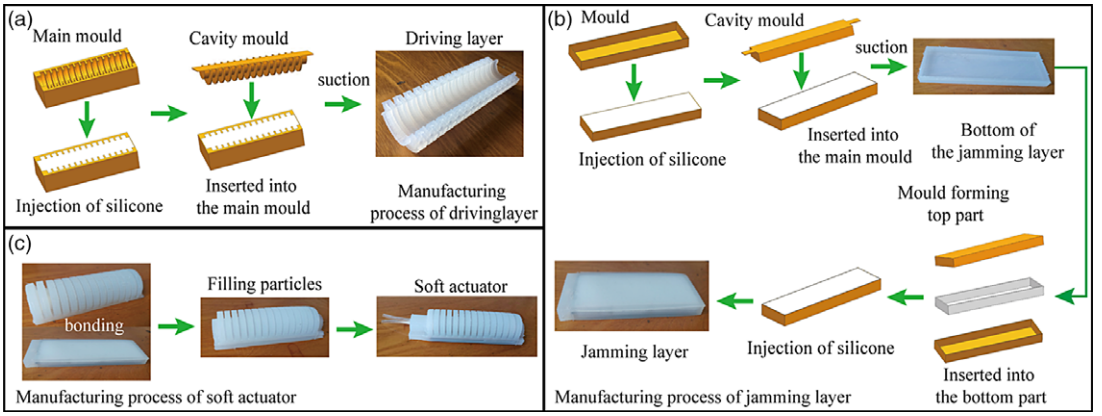

Figure 2. *A fabrication process of the soft actuator. (a) The manufacturing process of the driving layer. (b) Manufacturing of jamming layer. (c) Combination process of the actuator.*

move to a small extent as subjecting to external force. In this case, the actuator exhibits high stiffness. As shown in Fig. 1(c), there are two working modes. The first mode is the bending way. When the jamming layer is vacuum off, and the driving layer is inflated and pressurized, the actuator could be bending. In this way, the actuator exhibits low stiffness and flexibility to achieve significant bending. The second way is called rigidity mode. In this way, the actuator exhibits high load capacity. Via switching between jamming states, the actuator can behave either like a flexible member with low bending stiffness or like a stiff one with high stiffness.

2.2. Fabrication of actuator

The actuator was fabricated from highly elastic silicone rubber using a casting molding process. Since the driving layer has a multi-cavity structure, a driving and jamming layers were fabricated separately. The driving layer and the jamming layer are bonded to form an actuator. The actuator was made of 30-degree hardness and ordinary AB-type two-component silicone rubber. The specific manufacturing process of the actuator is shown in Fig. 2.

3. Bending performance analysis of actuator

3.1. Theoretical model

To illustrate the large-deformation capability of the actuator, we established the model describing the relationship between the air pressure and the bending angle. The soft actuator was fabricated using silicone rubber. We employed an incompressible Neo-Hookean model to describe its mechanical behavior. The strain energy is given by:

$$W = C_{10}(I_1 - 3) \tag{1}$$

where I_1 is the first invariant of the stress tensor, $I_1{=}\lambda_1^2 + \lambda_2^2 + \lambda_3^2$, λ_1, λ_2,λ_3 is axial, circumferential, and radial principal stretch ratio, respectively. $C_{10} = \frac{G}{2}$, where $G$is shear modulus of the material. The principal stress could be expressed as a function of W, λ_i, and the Lagrange multiplier p:

$$\sigma_i = \frac{\partial W}{\partial \lambda_i} - p\lambda_i^{-1} \tag{2}$$

Due to constraint of the jamming layer, the circumferential principal stretch is negligible, so that $\lambda_2 = 1$. Furthermore, the material is incompressible, thus $\lambda_1\lambda_2\lambda_3 = 1$. The principal stretch along each

https://doi.org/10.1017/S0263574721001740 Published online by Cambridge University Press

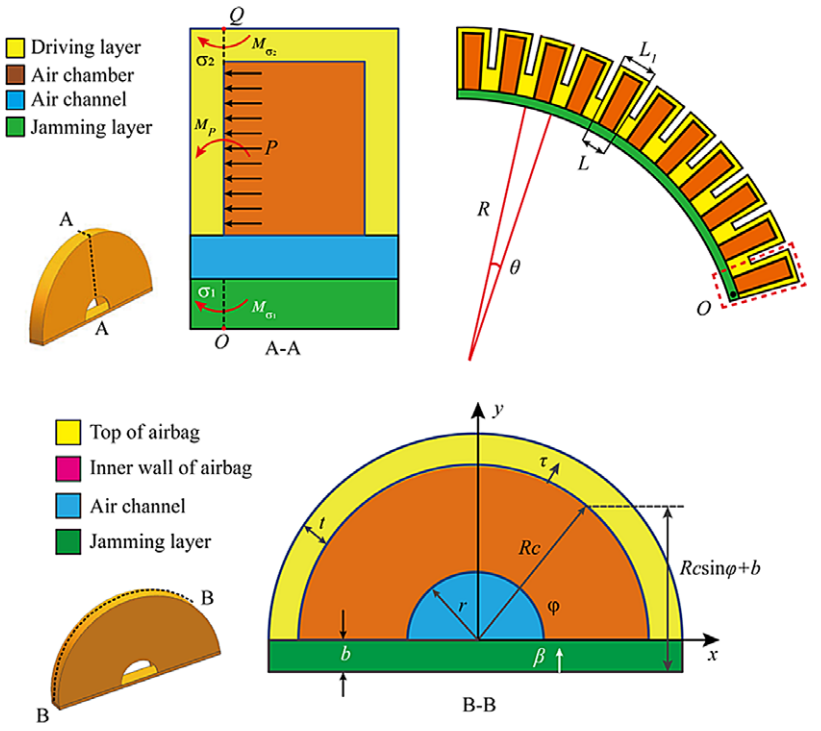

Figure 3. *Force analysis of one of air cavity.*

direction can be obtained that

$$\lambda_1=\lambda,\ \ \lambda_2=1,\ \ \lambda_3=\frac{1}{\lambda} \tag{3}$$

The principal stress can be given by combining Eqs. (1)–(3).

$$\begin{cases} \sigma_1=\dfrac{\partial W}{\partial \lambda_1}-p\lambda_1^{-1}=\dfrac{G}{2}\left(\lambda-\dfrac{1}{\lambda^3}\right) \\ \sigma_2=\dfrac{\partial W}{\partial \lambda_2}-p\lambda_2^{-1}=\dfrac{G}{2}\left(\lambda-\dfrac{1}{\lambda^2}\right) \\ \sigma_3=\dfrac{\partial W}{\partial \lambda_3}-p\lambda_3^{-1}=0 \\ p=\dfrac{C_{10}}{2}\lambda_3^2=\dfrac{C_{10}}{2\lambda^2} \end{cases} \tag{4}$$

The stretch λ is within the range of $1 \le \lambda \le 1.5$ considered in bending deformation of the actuator. The principal stress σ_2 is significantly smaller than σ_1. Therefore, the stress σ_1 is the only principal stress to be considered.

Here, we only consider the static mechanical behavior of the soft actuator and set the air pressure inside the air chamber to be the same. Therefore, one of the air cavities was selected for force analysis as shown in Fig. 3. The torque at the inner wall of the air cavity generated by the air pressure denotes M_p. M_{σ_1} is the torque from internal stress at the top of the driving layer and the bottom restraining layer. M_{σ_2}represents the torque induced by the internal stress of the driving layer at the top of the airbag. According to the torque balance, the following equation can be obtained as:

$$M_p = M_{\sigma_1} + M_{\sigma 2} \tag{5}$$

https://doi.org/10.1017/S0263574721001740 Published online by Cambridge University Press

The torque M_p can be expressed as:

$$M_p = 2P \int_0^{\frac{\pi}{2}} (R_c \sin\varphi + b) R_c^2 \cos^2\varphi d\varphi \tag{6}$$

where R_c is the radius of the air chamber, φ is the rotation angle, b is the thickness of jamming layer, and P is the air pressure.

Similarly, the torque M_{σ_1} and the torque M_{σ_2} can be expressed as:

$$M_{\sigma 1} = \int_0^b 2\sigma_1 (R_c + t) L\beta d\beta \tag{7}$$

$$M_{\sigma 2} = 2\int_0^t \left\{ \int_0^{\frac{\pi}{2}} \sigma_\tau [(R_c + \tau)^2 \sin\varphi + b(R_c + \tau)] L d\varphi \right\} d\tau \tag{8}$$

where t is the thickness of the driving layer and σ_τ is the tensile stress.

The longitudinal stretch and strain in the jamming layer can be obtained as (see Fig. 3):

$$\lambda_\beta = \frac{\beta + R}{R} = \frac{\beta + L/\theta}{L/\theta} = \frac{\beta\theta}{L} + 1 \quad \sigma_1 = \frac{C_{10}}{2}\left(\lambda_\beta - \frac{1}{\lambda_\beta^3}\right) \tag{9}$$

Similarly, the stretch and strain for the top layer is

$$\lambda_\tau = \frac{R + b + (R_c + \tau)\sin\varphi}{R} \quad \sigma_2 = \frac{C_{10}}{2}\left(\lambda_\tau - \frac{1}{\lambda_\tau^3}\right) \tag{10}$$

By substituting Eqs. (6)–(8) into Eq. (5), a relationship between the input air pressure and the bending angle can be obtained:

$$P = \frac{6\,[M_{\sigma 1}(\theta) + M_{\sigma 2}(\theta)]}{4{R_c}^3 + 3\pi {R_c}^2 + b} \tag{11}$$

3.2. Motion performance analysis

To demonstrate the motion performance of the actuator, we applied a pressure range of [0–45] kPa to test its bending angle. The theoretical, simulated, and experimental results of the bending angle under various air pressures are shown in Fig. 4(b). Our experiments and theoretical results show agreement and indicate the potential role of predictive motion characteristics for soft actuator design. The experimental measurement results are relatively accurate compared to theoretical and simulation results, because the experiment reflects the bending angle of the actuator under real conditions. It can be seen from the Fig. 4(b) that the theoretical and simulation results are different from the experimental values. The main reasons for the difference between simulation, theoretical models, and experimental results are as follows: (1) the silicone material parameters used in the simulation and theoretical model are obtained by fitting the experimental data measured through the tensile test, and there are errors with actual material; (2) the incompressible Neo-Hookean model adopted in this paper cannot accurately describe the super-elastic properties of silica gel; and (3) the gravity do not take into account in the simulation and theoretical model. The bending angle varies linearly with the air pressures. Furthermore, the bending angle is 224° at the air pressure of only 45 kPa. It was shown that relatively low pressure could gain a significant bending deformation, exhibiting the excellent motion feature of the presented soft actuator.

To capture the effects of the structural parameters on the motion performance of the actuator, we analyzed the bending angle variation from analytical and FEM modeling results (using software ANSYS). Poisson's ratio is set as 0.48, Young's modulus 2.25 MPa, and the density 1200 kg/m [3]. The Mooney–Rivlin second-order model in simulation software ANSYS is used to describe the mechanical properties of the silicone hyper-elastic material. The material constants associated with silica gel C_{10} is 0.18 MPa and C_{01} is 0.09 MPa. The tetrahedral element is applied to divide the mesh. The air pressures are exerted perpendicularly to the air channel. According to Eq. (8), the bending angle is associated with these

https://doi.org/10.1017/S0263574721001740 Published online by Cambridge University Press

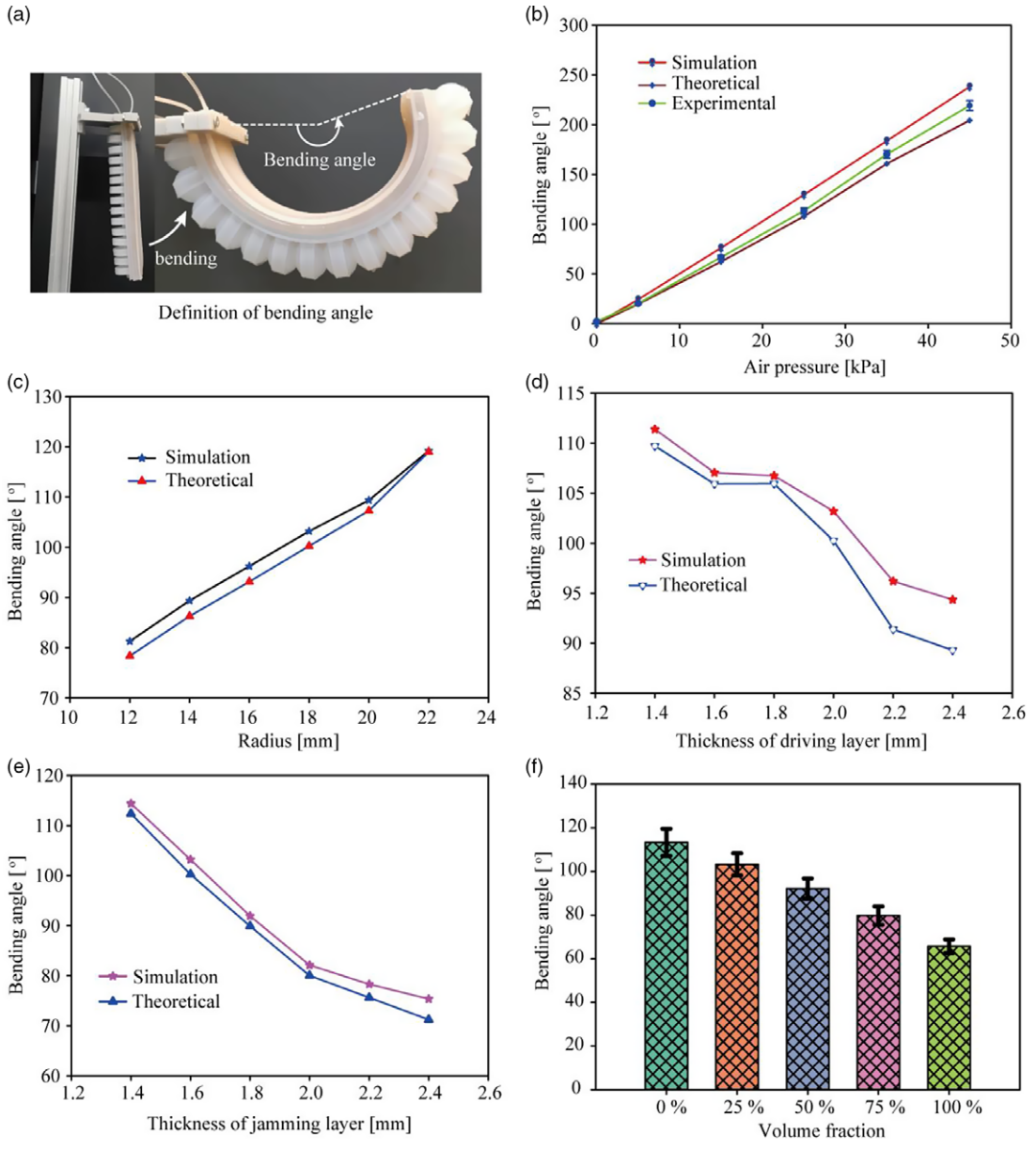

Figure 4. *Relationship between bending angle and air pressure, structural parameters, and volume fraction.*

parameters, such as radius of the air chamber, thickness of jamming layer, and thickness of driving layer. We measured the bending angle for parametersR_c, t_r, and t_a ranging from 10 to 24 mm, 1.2 to 2.6 mm, 1.2 to 2.6 mm, and maintaining the air pressure 20 kPa. The results showed that as the air chamber radius increases, the bending angle increases. The reason is that the larger the air cavity is, the greater the tensile deformation is under the same air pressure. Similarly, thicker driving and jamming layers limit the tensile deformation, resulting in a smaller bending angle. Therefore, the desired bending angle and motion range can be obtained by reasonably designing its parameters.

Due to the jamming layer bonded with the driving layer, we investigated how the compactness of particles inside the jamming structure affects the actuator's bending deformation. The compactness can

https://doi.org/10.1017/S0263574721001740 Published online by Cambridge University Press

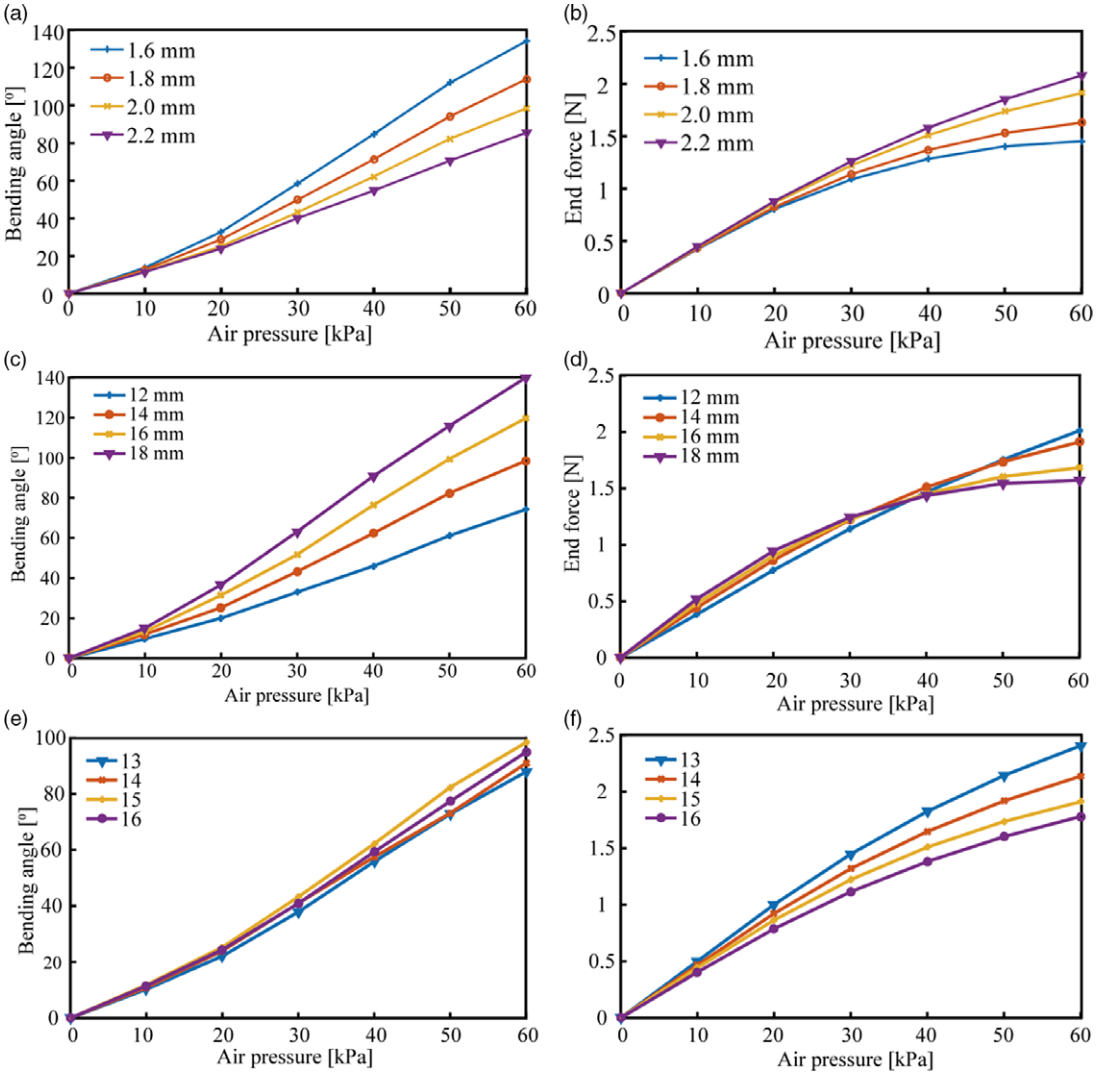

Figure 5. *Bending angle and end force of the soft actuator with different air pressure levels.*

be described with the volume fraction of granules. We experimentally tested the bending angle with volume fraction ranging from 0 to 100%, and the results are illustrated in Fig. 4(f). To demonstrate only the influence of the volume fraction, we set it to the same certain air pressure 25 kPa that does not affect the analytical results. The results showed that the maximum margin of the bending angle is up to 58^0 in no particles and wholly filled with granules. It reveals that the filling degree of particles significantly affects the motion characteristics of the soft actuator. Because the compactness of particles represents the higher stiffness of the jamming layer, it is difficult for the driving layer to bend. Thus, the stiffness and bending performance of the actuator are contradictory and need to be a trade-off.

Figure 5(a) and (b) show the bending angle and end force with different air pressure levels under different thickness of driving layer. From these figures, we can find that as the thickness increases, the bending angle decreases, but the end force increases. This shows that these mechanical properties are contradictory. To obtain a specific mechanical performance for the soft actuator, we need to tailor the structural parameters. When the thickness is 1.8 mm, the end force of the actuator has no significant change, but the force still has a significant increase when it is 2.0 mm. Meanwhile, we consider that the

https://doi.org/10.1017/S0263574721001740 Published online by Cambridge University Press

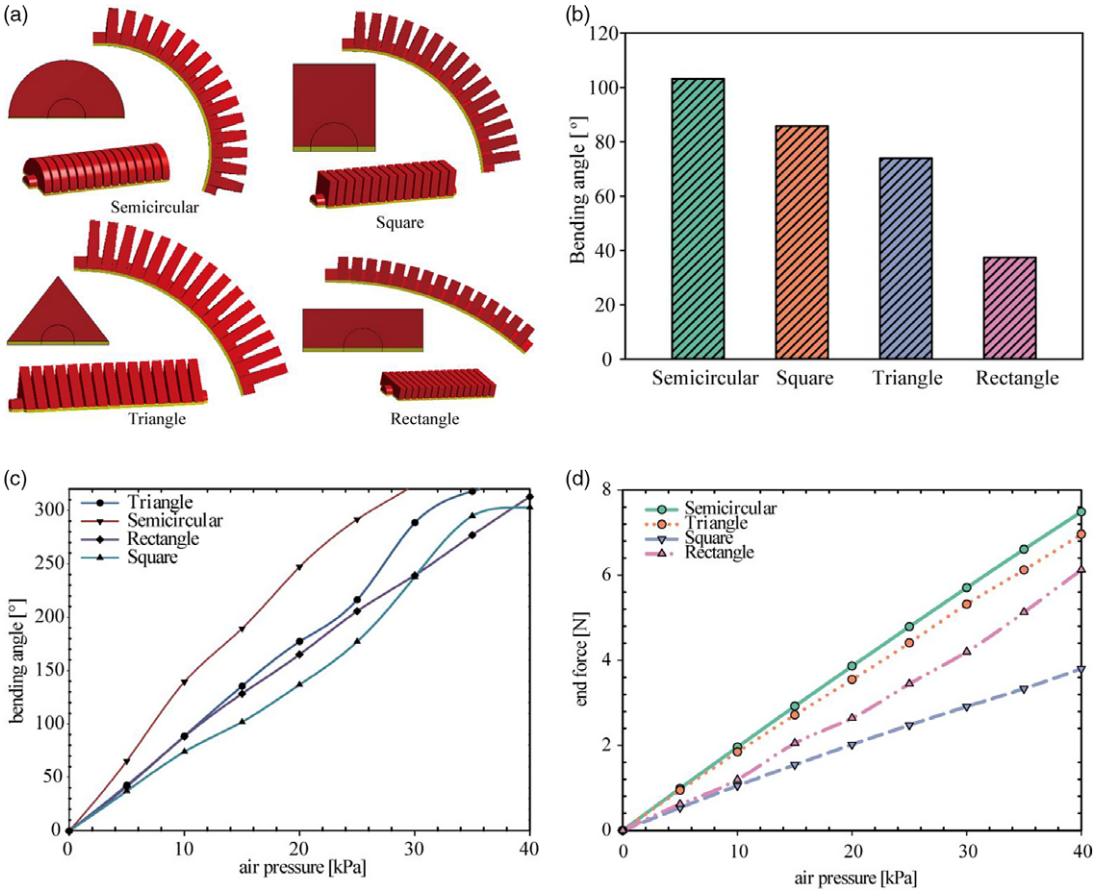

Figure 6. *Comparison of four actuators for bending performance. (a) Structural. (b) Bending angles of various chamber section shapes. (c) The relationship between bending and air pressure. (d) The relationship between end forces and air pressure.*

bending angle can be up to above 70^0 under the air pressure 100 kPa; thus, the thickness of the driving layer is determined as 2 mm. Similarly, the Fig. 5(c) and (d) illustrate the performance difference with the radius of the air chamber. The radius has less influence on end force but has significant effect on the bending angle. Thus, the radius is set as 18 mm. The number of air chamber can also result in the difference between bending angle and end force as shown in Fig. 5(e) and (f). The number of the air chamber has little effect on the bending angle, but great effect on the end force. With the number increases, the end force decreases. The number of air chamber is determined as 13. Thus, the bending angle and output force of the actuator are contradictory and need to be a trade-off. A comparative analysis method was employed to optimize the structural parameters of the soft actuator for functional specifications.

We demonstrated good motion performance by comparing three actuators with various chamber section shapes, such as rectangular, triangular, and square. We assumed the same structural parameters (the lengths, air channel radius, thickness, and volume) of the four actuators. Because the air pressure in each air chamber is greater than that in the outside, the difference of air pressure causes the expansion of the air chamber. This enables adjacent air chambers to press against each other, resulting in tensile deformation of the driving layer. But the jamming layer does not stretch, causing the actuator bend. Therefore, the bending angle of the soft actuator depends on expansion deformation of each air chamber. Figure 6 illustrates the expansion deformation with different section shapes. The air pressure is 20 kPa for measuring the corresponding bending angle (see Fig. 6(b)). The experimental results demonstrated that the

https://doi.org/10.1017/S0263574721001740 Published online by Cambridge University Press

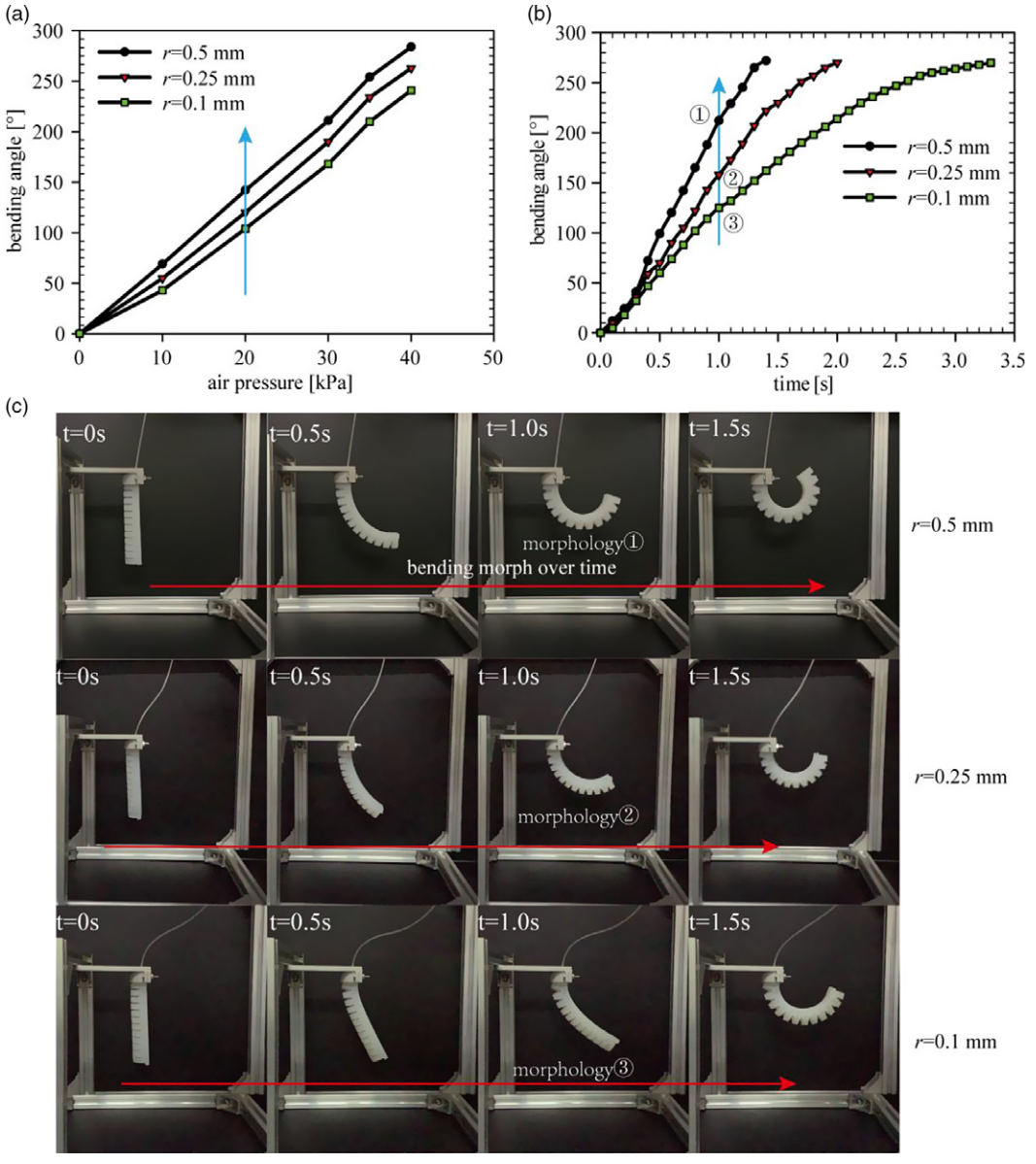

Figure 7. *Influence of air pipeline radius. (a) Influence of the pipeline radius on bending angle. (b) Bending angle over time with various radius. (c) Demonstration of bending morphology variation.*

designed actuator with a semicircular air chamber has a significantly larger bending angle than the other actuators. Figure 6(c) and (d) show the bending angle and end force with different air pressure levels. The actuator with semicircular section shape has better bending and force output compared with other three section shapes. This further demonstrates that the proposed soft actuator has better mechanical performance.

Furthermore, we investigated the dependence of gas pipeline radius r (see Fig. 3) on bending angle and bending morph over time. Figure 7(a) shows the bending angle with the small pipeline radius of 0.5, 0.25, and 0.1 mm. As can be seen from the figure, the bending angle could decrease as the radius decreases. The smaller pipeline radius increases the flow resistance inside air chamber, resulting in

https://doi.org/10.1017/S0263574721001740 Published online by Cambridge University Press

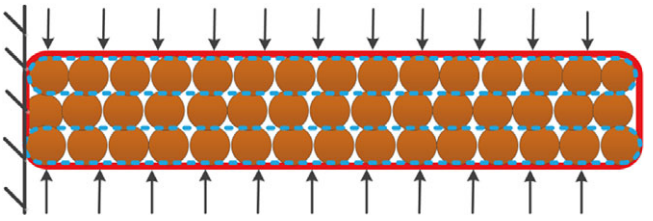

Figure 8. *Equivalent model of jamming layer.*

bending morph variation. Figures 7(b) and 6(c) illustrated the bending morph changes over time with various pipeline radii. The actuator has a different motion pattern at a certain time under the same pressure. For example, the morphology varies at time 1 s as shown in Fig. 7(c). Therefore, the actuator has various morphologies during its motion, especially in the case of relatively small air pipe diameters.

4. Stiffness characteristics of the actuator

4.1. Influence factors of actuator stiffness

As shown in Fig. 8, the jamming layer is equivalent to a cantilever structure composed of multilayer granules as it is subjected to vacuum pressure. When an external force F_{i} is applied at the end of the jamming layer, the displacement of the end d_{o} is generated, and the stiffness of the jamming layer can be expressed as:

$$k = \frac{F_{\mathrm{i}}}{d_{\mathrm{o}}} \tag{12}$$

It can be seen from formula (12) that when the external force F_{i} is constant, the end displacement d_{o} is smaller, the higher the jamming layer stiffness is. From the energy point of view, the work done by the external force is transformed into the elastic strain energy of the jamming layer and the energy loss caused by the friction between the granules of each layer, which can be expressed as:

$$W_{\mathrm{F}} = F_{\mathrm{i}} d_{\mathrm{o}} = U + W_{\mathrm{s}} \tag{13}$$

where W_{F} represents the work done by the external force, W_{s} is the energy loss due to the friction between the granules, and U is the elastic strain energy.

Equation (13) shows that the larger the energy loss is, the smaller the elastic strain energy is. And the smaller the displacement of the end of the jamming layer is, the higher the rigidity of the jamming layer is. The stiffness of the jamming layer is mainly affected by the energy loss caused by the friction between granules, and the friction energy loss between the granules of each layer can be expressed as:

$$W_{\mathrm{s}} = nfd_s = n\mu F_n d_s \tag{14}$$

where f is the friction between the layers of granules, d_s is the sliding displacement of each layer of granules, and n is the number of layers of granules. μ and F_n are the friction factor and the normal force between the granule layers. When the jamming layer is in a vacuum state, the normal force between the granules is

$$F_n = \Delta P s \tag{15}$$

where ΔP is the vacuum inside the flexible strip, and s is the surface area between the jamming granules and the flexible membrane.

The relationship between the number of granule layers n and the volume fraction of jamming granules is

$$n = c_1 \varphi_z \tag{16}$$

where c_1 is the proportionality factor.

https://doi.org/10.1017/S0263574721001740 Published online by Cambridge University Press

The jamming granule volume fraction φ_z represents the ratio of the jamming granule volume V_z to the flexible strip volume V_r in the normal state:

$$\varphi_z = \frac{V_z}{V_r} \tag{17}$$

Substituting Eqs. (12)–(15) into Eq. (11), the friction energy loss is

$$W_s = \frac{c_1 \mu \Delta P s d_s V_z}{V_r} \tag{18}$$

The friction factor μ is related to the size, shape, and surface roughness of the jamming granules [28, 29]. According to Eq. (16), the stiffness of the actuator is related to the size of the jamming granules, the volume fraction, the shape, the roughness of the surface, and the internal vacuum of the jamming layer.

4.2. Stiffness performance analysis

We aim to investigate the actuator's stiffness variation with granule magnitude, shape, surface roughness, and volume fraction. The experimental setup is shown in Fig. 9(a) to measure the stiffness of the soft pneumatic actuator. We used a weight of 300 g acting on the end of the actuator and measured the corresponding displacement using a laser interferometer. The stiffness at the position can denote the ratio between the load and the displacement. The smooth spheroidal glass sand (see Fig. 9(b)) with diameters of 1, 3, and 5 mm are used to analyze the effect of granule magnitude on the stiffness (Fig. 9(c)). The double star indicates that different particle diameters have a significant difference in stiffness. The experimental results showed the smaller the granule diameter is, the greater the stiffness of the actuator is. The smaller granules increase their contact area, resulting in greater friction and stiffness. To illustrate the influence of granule shapes, we compared the stiffness of two conditions of particles with spherical and cube. Because of the large contact area between cubic granules, the actuator filled with cubic granules exhibits higher stiffness than spherical granules. Granule surface roughness has impact on the contact friction, and two types of jamming layers filled with particles of different relative roughness were used to show their varied stiffness. Obviously, the actuator with rough granules has a higher stiffness, because the coarse granules have a higher friction factor.

To illustrate the effect of granule volume fraction on the stiffness, we filled the jamming layer with volume fractions of 20%, 40%, 60%, 80%, and 100%, respectively. Figure 9(d) shows that the increased stiffness is up to 100 N/m, compared with the volume fraction of 20% and 100%. This indicates that the compactness of the jamming layer has a significant influence on the stiffness because of the increase of its friction. As mentioned earlier, jamming of granular media needs to subject to a specific level of vacuum pressure. We explored how various levels of stress impact the stiffness and set the negative pressure range of [0 ∼ -25] kPa. Figure 9(e) shows the stiffness variation under different vacuum pressure. With the increase in vacuum pressure, the stiffness increases rapidly, but the stiffness varies slowly once the pressure is above 15 kPa. Therefore, the stiffness cannot be entirely regulated by vacuum pressure.

Furthermore, we want to understand whether the stiffness varies under a specific negative pressure when the actuator bends to different angles. The air pressure range of [10–50] kPa is applied to the driving layer to bend different angles. As can be seen from Fig. 9(f), the stiffness changes slightly at different bending angles, indicating that the actuator's stiffness has a good consistency during its motion process.

To demonstrate the dynamic feature of the soft actuator, we constructed an experimental setup (Fig. 10(a)) to test its dynamic response subjected to a square-wave air pressure, which is obtained by using relays and solenoid valve sets. It is inflated at period t_1, and it is deflated at time slot t_2. The square-wave air pressure (duty ratio 50%) with different frequencies indicates various inflating and deflating time. Figure 10(b) described the vibrational process of the soft actuator as the square-wave air pressure with period of 1, 2, 4, and 8 s are applied. By comparing these figures in Fig. 10(b), we can find the following differences as the period T increases. (1) The number of oscillations of the actuator reduces with

https://doi.org/10.1017/S0263574721001740 Published online by Cambridge University Press

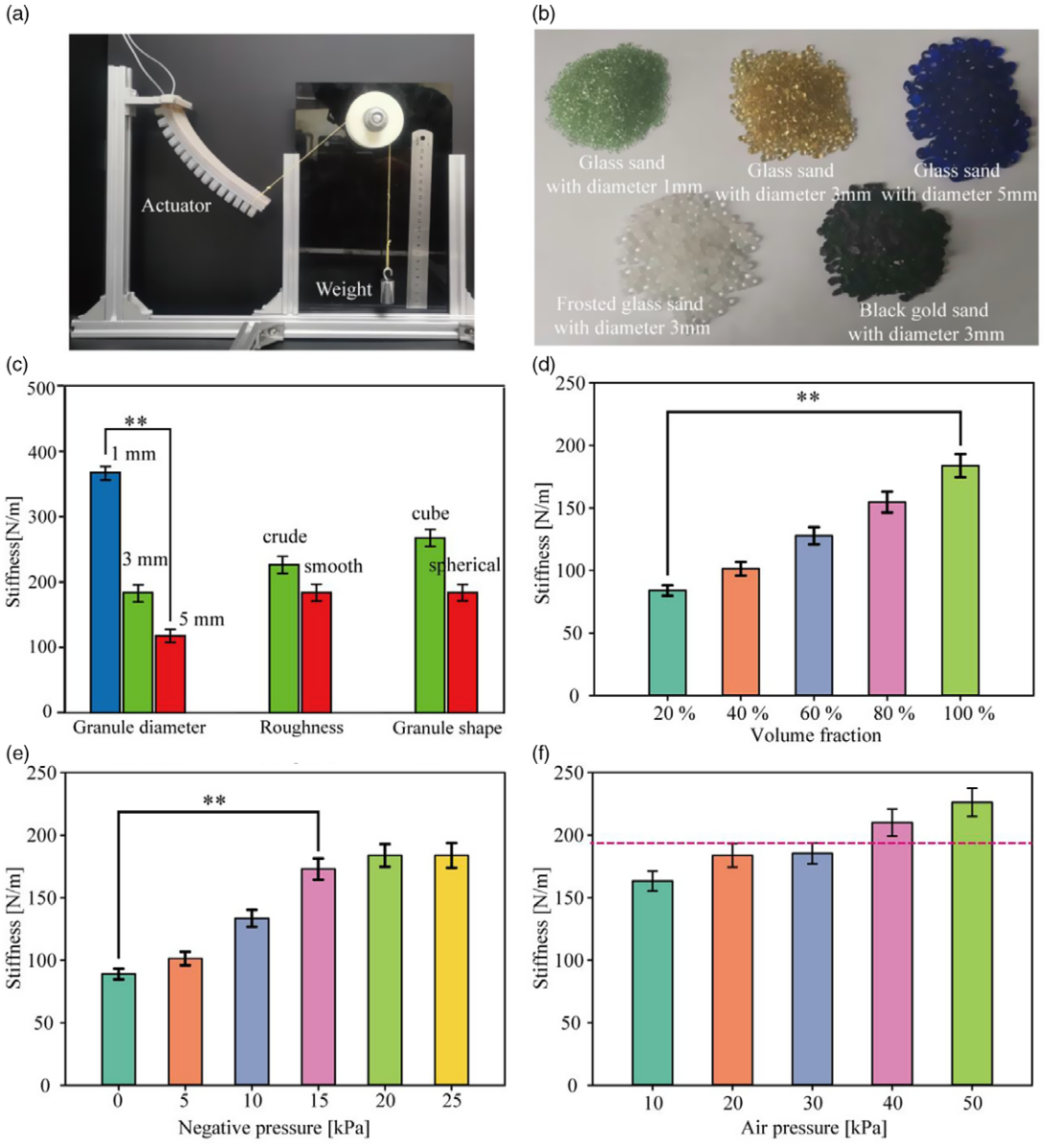

Figure 9. *Stiffness test of the actuator. (a) Experimental setup. (b) Granules filled in the actuator. (c) Grab testing of different objects. (d) Relationship between stiffness and volume fraction. (e) Relationship between stiffness and negative pressure. (f) Stiffness under various bending angle.*

the increase of the period. (2) Because the square-wave air pressure is applied, the steady-state response is bending back and forth. A red dotted box indicates the steady-state response in Fig. 10(b). The transient process time decreases with the increase of the period. (3) The amplitude of steady-state vibration increases with the increase of period. The reason for this difference is that the rheological properties of the soft actuator vary from different dynamic air pressure. Therefore, the soft actuator exhibits mechanical properties at dynamic pressure that are different from those at static pressure. The soft actuator exhibits different transient and steady vibration behavior when the jamming layer is vacuum off or vacuum on. From the transient response, the actuator with greater stiffness needs more time to reach steady

https://doi.org/10.1017/S0263574721001740 Published online by Cambridge University Press

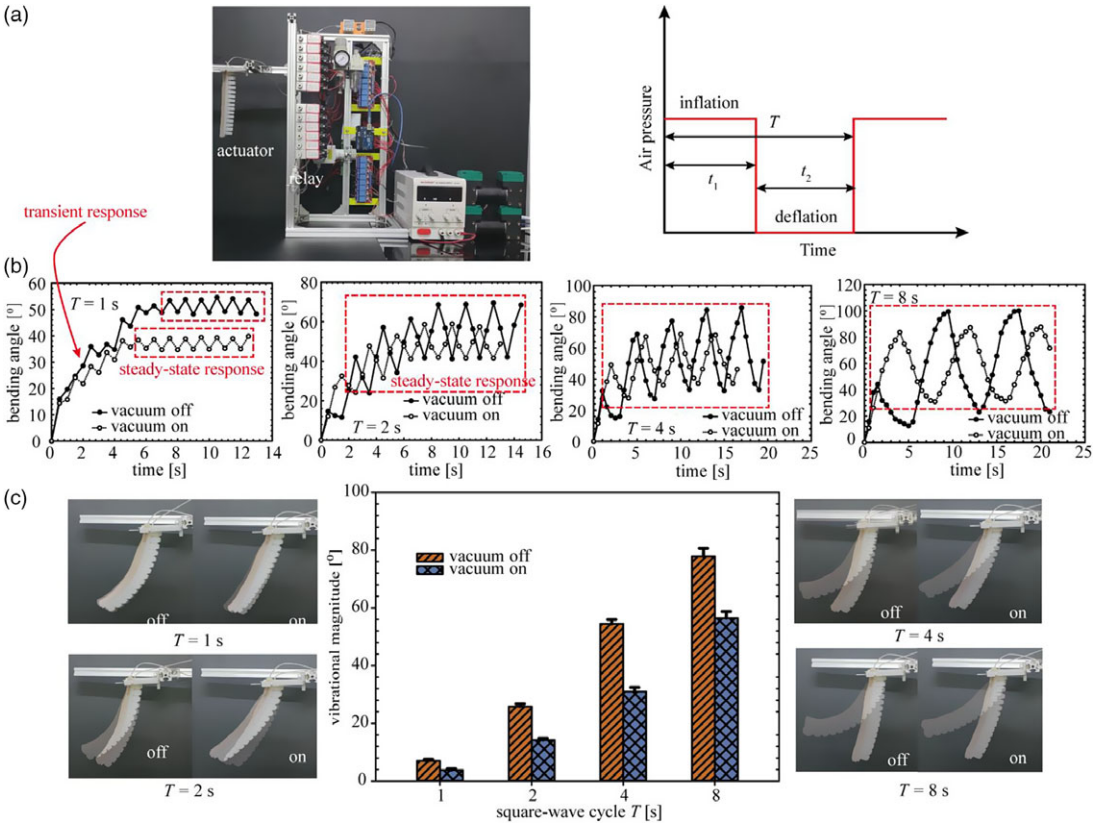

Figure 10. *Vibration performance of the soft actuator under square-wave air pressure. (a) Experimental setup. (b) Vibration process of the soft actuator with various periods. (c) Comparison of effects of stiffness on vibrational magnitude.*

state, which means it is more responsive. But when it stabilizes, a more rigid actuator has a smaller range of motion (see also from Fig. 10(c)), that is, the amplitude of its swing is smaller. Furthermore, we analyzed the vibrational magnitude with various frequency and stiffness variation. The larger the vibration frequency (the smaller the period), the smaller the amplitude of the actuator's vibration. The difference of vibration magnitude in vacuum and non-vacuum state is determined by the vibration frequency. This dynamic performance provides support for us to design soft robot using this soft actuator.

4.3. Variable stiffness test

To show the potential advantage of stiffness variety, we carried out two sets of experiments to demonstrate the carrying capacity and adapt autonomously to different shapes. We compared the maximum mass that can be grabbed using the soft actuator with vacuum on and off (see Fig. 11(a)). Figure 11(b) shows the load-bearing capability of the actuator with different negative pressure. As the negative pressure increases, the weight that can be sustained increases. The actuator can bear up to 700 g when the negative pressure is −60 kPa. The actuator can sustain the weight up to 1.39 kg, and it showed that the effect of stiffness change is evident. It shows that the particle jamming method has better load-bearing capacity compared to SMP [30]. Meanwhile, our proposed variable stiffness method can achieve the change of stiffness by applying different negative pressure. We demonstrate that the actuator grasps a variety of objects (Fig. 11(c)) by this way of pinching grasp and conforming to objects. It shows that the actuator has strong adaptability and can adjust the stiffness in terms of different shapes, sizes, and

https://doi.org/10.1017/S0263574721001740 Published online by Cambridge University Press

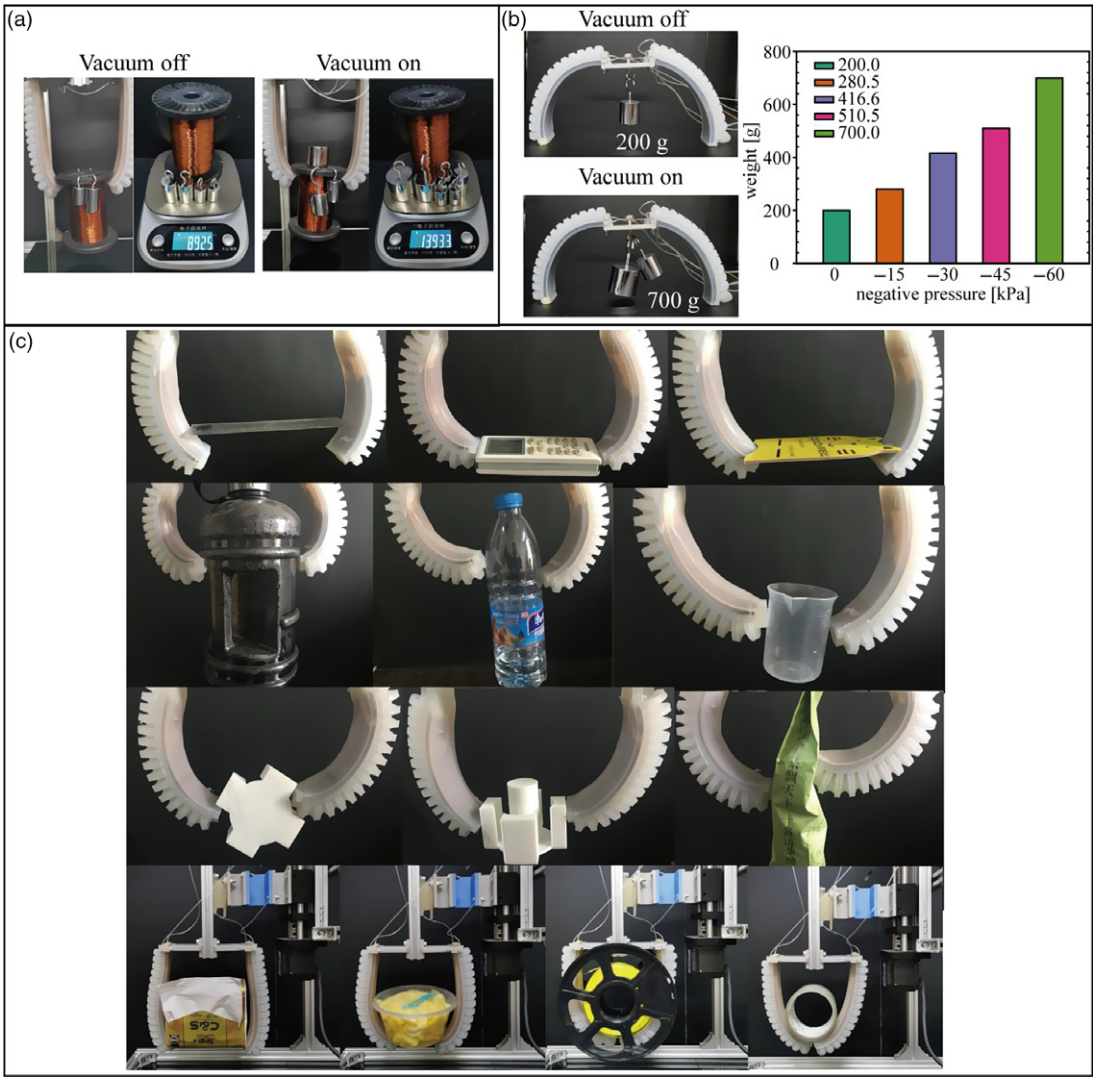

Figure 11. *Demonstration of stiffness variation of the actuator. (a) Maximum weight that can be grabbed. (b) Load-bearing capacity test. (c) Grabbing different objects.*

masses of objects. The soft actuator exhibits the ability to manipulate delicate objects and to undergo large deformation. And the compliance of the actuator allows it conforms to different shapes.

5. Conclusions

In this paper, a novel type of soft actuator with a large-bending angle and variable stiffness was constructed using granular jamming. A fast pneumatic net structure boned with a membrane filled with granules was designed to vary its stiffness. A theoretical model reflecting the motion performance of the actuator was established to analyze the influence of structural parameters on the bending performance of the actuator. The results showed that the designed actuator has a larger bending angle than the conventional counterpart, and the angle can reach 224 degrees at a pressure of 45 kPa. Furthermore, we investigated the dependence of air pipeline on bending angle and morphology during its motion. The

https://doi.org/10.1017/S0263574721001740 Published online by Cambridge University Press

flow resistance inside air chamber results in bending morphology variation. The influence factors of stiffness variation of the actuator were illustrated from energy of point of view. The actuator's stiffness variations with granule magnitude, shape, surface roughness, and volume fraction were investigated. The principle and essence of the stiffness variation of the actuator were described experimentally and theoretically. Meanwhile, we demonstrated the dynamic characteristics of the actuator with stiffness variation and analyzed their mutual restriction relationship. These conclusions provide a basis for us to capture its kinematic, dynamic, and stiffness. Future work will focus on theoretically establishing the dynamic mechanical model under negative pressure to reveal the behavior of dynamic damping and stiffness of the soft actuator. Moreover, the future research attention will focus on new applications of this soft actuator, including soft robots, compliant mechanisms, and bio-mimetics robots.

Acknowledgments.

Financial Support. This work is supported by the National Natural Science Foundation of China (Grant Nos. 51865016, 51565016), Natural Science Foundation of Jiangxi Province – Key Project (Grant No. 2020ACBL204009), Science and the Program of Qingjiang Excellent Young Talents, Jiangxi University of Science and Technology (Grant No. JXUSTQJBJ2018006).

Supplementary Material. To view supplementary material for this article, please visit https://doi.org/10.1017/S0263574721001740.

References

[1] K. Suzumori, S. Iikura and H. Tanaka, "Development of Flexible Microactuator and its Applications to Robotic Mechanisms," *Proceedings. IEEE International Conference on Robotics and Automation* (IEEE Computer Society, 1991).
[2] D. Rus and M. T. Tolley, "Design, fabrication and control of soft robots,"*Nature* **521**, 467–475 (2015).
[3] C. Laschi, B. Mazzolai and M. Cianchetti, "Soft robotics: Technologies and systems pushing the boundaries of robot abilities,"*Sci. Rob.* **1**(1), eaah3690 (2016).
[4] S. I. Rich, R. J. Wood and C. Majidi, "Untethered soft robotics," *Nat. Electron.* **1**(2), 102–112 (2018).
[5] D. Jeong and K. Lee, "Design and analysis of an origami-based three-finger manipulator," *Robotica* **36**(2), 261–274 (2018).
[6] N. Kastor, R. Mukherjee, E. Cohen, V. Vikas, B. A. Trimmer and R. D. White, "Design and manufacturing of tendon-driven soft foam robots," *Robotica* **38**(1), 88–105 (2020).
[7] G. Bao, L. Chen, Y. Zhang, S. Cai, F. Xu, Q. Yang and L. Zhang, "Trunk-like soft actuator: design, modeling, and experiments," *Robotica* **38**(4), 732–746 (2020).
[8] C. S. Haines, M. Lima, N. Li, G. M. Spinks, J. Foroughi, J. Madden, S. Kim, S. Fang, M. Andrade, F. Göktepe, Ö. Göktepe, S. Mirvakili, S. Naficy, X. Lepro, J. Oh, M. Kozlov, S. Kim, X. Xu, B. Swedlove, G. Wallace and R. Baughman, "Artificial muscles from fishing line and sewing thread," *Science* **343**(6173), 868–872 (2014).
[9] A. Firouzeh, M. Salerno and J. Paik, "Soft Pneumatic Actuator with Adjustable Stiffness Layers for Multi-Dof Actuation," *2015 IEEE/RSJ International Conference on Intelligent Robots and Systems (IROS)* (IEEE, 2015).
[10] A. Tonazzini, S. Mintchev, B. Schubert, B. Mazzolai, J. Shintake and D. Floreano, "Variable stiffness fiber with self-healing capability," *Adv. Mater.* **28**(46), 10142–10148 (2016).
[11] Y. Haibin, C. Kong, J. Li and G. Yang, "Modeling of grasping force for a soft robotic gripper with variable stiffness," *Mech. Mach. Theory* **128**, 254–274 (2018).
[12] C. Majidi and R. J. Wood, "Tunable elastic stiffness with micro confined magnetorheological domains at low magnetic field," *Appl. Phys. Lett.* **97**(16), 164104 (2010).
[13] N. G. Cheng, A. Gopinath and L. Wang, "Thermally tunable, self-healing composites for soft robotic applications," *Macromol. Mater. Eng.* **299**(11), 1279–1284 (2014).
[14] Y. F. Zhang, N. B. Zhang and H. Hardik, "Fast-response, stiffness-tunable soft actuator by hybrid multilateral 3D printing," *Adv. Funct. Mater*. **29**(15), 1806698 (2019).
[15] F. Alambeigi, R. Seifabadi and M. Armand, "A Continuum Manipulator with Phase Changing Alloy," IEEE International Conference on Robotics and Automation (2016) pp. 758–764.
[16] Y. Wei, Y. Chen, T. Ren, Q. Chen, C. Yan, Y. Yang and Y. Li, "A novel, variable stiffness robotic gripper based on integrated soft actuating and particle jamming," *Soft Rob.* **3**(3), 134–143 (2016).
[17] Y. Li, Y. Chen, Y. Yang and Y. Wei, "Passive particle jamming and its stiffening of soft robotic grippers," *IEEE Trans. Rob.* **33**(2), 446–455 (2017).
[18] Y. S. Narang, J. J. Vlassak and R. D. Howe, "Mechanically versatile soft machines through laminar jamming," *Adv. Funct. Mater.* **28**(17), 1707136 (2018).
[19] W. H. Choi, S. Kim, D. Lee and D. Shin, "Soft, multi-DoF, variable stiffness mechanism using layer jamming for wearable robots," *IEEE Rob. Autom. Lett.* **4**(3), 2539–2546 (2019).

[20] J. R. Amend, E. Brown and N. Rodenberg, "A positive pressure universal gripper based on the Jamming of granular material," *IEEE Trans. Rob*. **28**(2), 341–350 (2012).
[21] E. Brown, N. Rodenberg and J. Amend, "Universal robotic gripper based on the jamming of granular material," *Proc. Natl. Acad. Sci. U.S.A*. **107**(44),18809–18814 (2010).
[22] A. J. Loeve, O. S. Ven and J. G. Vogel, "Vacuum packed particles as flexible endoscope guides with controllable rigidity," *Granular Matter* **12**(6), 543–554 (2010).
[23] Y. J. Kim, S. Cheng and S. Kim, "A novel layer Jamming mechanism with tunable stiffness capability for minimally invasive surgery," *IEEE Trans. Rob*. **29**(4), 1031–1042 (2013).
[24] T. Wang, J. Zhang, Y. Li, J. Hong and M. Y. Wang, "Electrostatic layer jamming variable stiffness for soft robotics," *IEEE/ASME Trans. Mechatron*. **24**(2), 424–433 (2019).
[25] J. Amend and H. Lipson, "The JamHand: Dexterous manipulation with minimal actuation," *Soft Rob.* **4**(1), 70–80 (2017).
[26] Y. Li, Y. Chen, Y. Yang and Y. Wei, "Passive particle jamming and its stiffening of soft robotic grippers," *IEEE Trans. Rob*. **33**(2), 446–455 (2017).
[27] Y. Wei, Y. Chen, Y. Yang and Y. Li, "A soft robotic with tunable stiffness based on integrated ball joint and particle jamming," *Mechatronics* **33**, 84–92 (2016).
[28] B. Mosadegh, P. Polygerinos and C. Keplinger, "Soft robotics: Pneumatic networks for soft robotics that actuate rapidly," *Adv. Funct. Mater.* **24**(15), 2109–2109 (2014).
[29] L. A. Abeach, S. Nefti-Meziani and T. Theodoridis, "A variable stiffness soft gripper using granular jamming and biologically inspired pneumatic muscles," *J. Biomimetic Eng*. **15**(2), 236–246 (2018).
[30] Y. Yang, Y. Chen, Y. Li, Michael, Z. Q. Chen and Y. Wei, "Bioinspired robotic fingers based on pneumatic actuator and 3D printing of smart material," *Soft Rob*. **4**(2), 147–162 (2017).

Cite this article: J. Hu, L. Liang and B. Zeng (2022). "Design, modeling, and testing of a soft actuator with variable stiffness using granular jamming", Robotica **40**, 2468–2484. https://doi.org/10.1017/S0263574721001740